

Increased High-frequency Oscillations Precede in vitro Low-Mg²⁺ Seizures

*Houman Khosravani, †C. Robert Pinnegar, †J. Ross Mitchell, ‡Berj L. Bardakjian,
*Paolo Federico, and §Peter L. Carlen

*Department of Clinical Neurosciences and the Hotchkiss Brain Institute, and †Department of Radiology, Seaman Family MR Research Centre, University of Calgary, Calgary, Alberta; and ‡Institute of Biomaterials & Biomedical Engineering, and §Toronto Western Research Institute, University Health Network, University of Toronto, Toronto, Ontario, Canada

Summary: *Purpose:* High-frequency oscillations (HFOs) in the range of ≥ 80 Hz have been recorded in neocortical and hippocampal brain structures in vitro and in vivo and have been associated with physiologic and epileptiform neuronal population activity. Frequencies in the fast-ripple range (> 200 Hz) are believed to be exclusive to epileptiform activity and have been recorded in vitro, in vivo, and in epilepsy patients. Although the presence of HFOs is well characterized, their temporal evolution in the context of transition to seizure activity is not well understood.

Methods: With an in vitro low-magnesium model of spontaneous seizures, we obtained extracellular field recordings (hippocampal regions CA1 and CA3) of interictal, preictal, and ictal activity. Recordings were subjected to power–frequency analy-

sis, in time, by using a local multiscale Fourier transform. The power spectrum was computed continuously and was quantified for each epileptiform discharge into four frequency ranges spanning subripple, ripple, and two fast-ripple frequency bands.

Results: A statistically significant increasing trend was observed in the subripple (0–100 Hz), ripple (100–200 Hz), and fast-ripple 1 (200–300 Hz) frequency bands during the epoch corresponding to the transition to seizure (preictal to ictal).

Conclusions: Temporal patterns of HFOs during epileptiform activity are indicative of dynamic changes in network behavior, and their characterization may offer insights into pathophysiologic processes underlying seizure initiation. **Key Words:** Ripples—Epilepsy—Time–frequency—Preictal.

Neuronal population activity recorded electrophysiologically in the range of ≥ 80 Hz is collectively referred to as high-frequency oscillations [HFOs (1)]. Waveforms with spectral components in the HFO range have been recorded in the hippocampus and entorhinal cortex in both normal (2–4) and epileptic neuronal networks (5–9). HFOs are further classified into two frequency bands: ripple (~ 100 –200 Hz) and fast ripple (FR, ≥ 200 Hz) bands. Cellular and network mechanisms underlying HFOs are believed to involve both excitatory and inhibitory synaptic transmission (10), in addition to electrotonic coupling (11). These modalities of coupling allow dynamic and transient changes in synchronization of subpopulations of neurons in larger networks (12). Recent evidence suggests that gap-junctions located between axons of hippocampal pyramidal cells can underlie high-frequency activity (13–16).

Under nonepileptic conditions, ripples may play a role in memory consolidation, transferring information from the hippocampus to the neocortex (17,18). Ripples and FRs also can coexist under epileptic conditions. They have been observed in the in vivo recordings of seizure-like activity and in intracranial EEG recordings from hippocampal and entorhinal cortices of epilepsy patients during video-EEG monitoring (5,6). Although HFOs in the ripple band are observed in both normal and epileptic states of brain activity, FRs are observed predominantly in seizure foci (7,8,19,20). Therefore FRs may serve as “surrogate markers” for the presence of an underlying epileptic condition (16,21). Thus identification and characterization of FRs, particularly during the preictal period (22), may be of clinical value. To date, few studies have quantitatively analyzed how HFOs evolve over time from interictal, preictal, and to ictal activity (23–25).

In this study, we quantified the temporal evolution of HFOs during the transition from interictal to ictal activity in a recurrent spontaneous (low-magnesium) model of epilepsy. Interictal, preictal, and ictal discharges were recorded extracellularly in the CA1 or CA3 cell layer of rat

Accepted April 12, 2005.

Address correspondence and reprint requests to Dr. P. Federico at Department of Clinical Neurosciences, University of Calgary, Room C1241A, Foothills Medical Centre, 1403-29th Street N.W., Calgary, AB, Canada T2N 2T9. E-mail: pfederic@ucalgary.ca

hippocampal brain slices. The recorded activity was visualized and quantified by using a local multiscale Fourier transform (LMS-FT), which permitted detailed power-frequency analysis of the electrophysiologic activity ranging from low to FR frequencies.

MATERIALS AND METHODS

Brain slices and solutions

Seven male Wistar rats (P21–24) were anesthetized with halothane and decapitated. The brain was quickly dissected and maintained in ice-cold artificial cerebrospinal fluid (aCSF) for 4–5 min. Brain slices were cut according to Rafiq et al. (26,27). After sectioning, slices were maintained at room temperature in oxygenated aCSF for ≥ 1 h before recording. The aCSF contained (in mM): NaCl, 125; KCl, 2.5; NaH_2PO_4 , 1.25; MgSO_4 , 2; CaCl_2 , 1.5; NaHCO_3 , 25; D-glucose, 10; pH 7.4 when aerated with 95% O_2 and 5% CO_2 . Osmolarity was 310 ± 5 mOsm. For electrophysiologic recordings, the superfusing aCSF was switched to one containing 5 mM KCl and 0.5 mM MgSO_4 , to ensure the development of spontaneous epileptiform activity (28,29). Twelve ($\sim 86\%$) of 14 slices developed interictal events that spontaneously progressed to seizure-like events (SLEs). The observed transition was consistent with previous reports using this model of epilepsy (28,30). Given that recurrent SLEs are observed in this model, we define an “episode” as encompassing a single interictal-to-ictal transition (Fig. 1A). For subsequent quantitative analysis, we used one slice from each of the seven animals that exhibited the aforementioned SLEs and analyzed the first five episodes from each slice. This selection was made to ensure consistency and viability across seizures from different slices. In total, 35 complete episodes were analyzed.

Electrophysiologic recordings

Brain slices were transferred to a superfusion chamber maintained at 35°C (SD, 2) (Medical Systems Corp., Greenvale, NY, U.S.A. Model PDMI-2) and superfused with the low- Mg^{2+} aCSF at a rate of 4 ml/min. Epileptiform discharges were observed within 10 to 20 min of perfusion with low- Mg^{2+} aCSF (Fig. 1A). Extracellular recordings were made by using an Axoclamp 2B amplifier (Molecular Devices Corp., Union City, CA, U.S.A.). Signals were first low-pass filtered (at 625 Hz, in-house built hardware eight-pole Bessel filter) and acquired at 2 KHz (Digidata 1322A; Molecular Devices Corp.) continuously. DC shifts were subtracted by a moving average filter corresponding to a high-pass frequency of 0.2 Hz. For the purpose of analysis, continuous data for each episode from each slice were segmented into two groups: interictal-to-preictal and ictal. Data were digitally notch filtered at 60, 180, and 300 Hz (± 3 Hz) to remove line noise. The recording electrodes were filled with NaCl (150 mM) and placed in the CA1 or CA3 cell body layer or both. For three of

the slices ($n = 15$ episodes), dual simultaneous CA1/CA3 or CA3/CA3 recordings were performed. A stimulating electrode was placed in the mossy fiber region. At approximately 1 min after the end of each seizure-like event (between episodes), single evoked field responses were used to monitor tissue viability, while waiting for spontaneous epileptiform discharges (EDs) to reappear. The intensity of stimulation was fixed for each experiment but varied between slices, adjusted to a value that evoked a single field potential in the CA1 layer.

Power spectral analyses

Power-frequency analysis of all recordings was performed continuously over time by using an LMS-FT (31). We have described its use analyzing medical imaging (multidimensional) magnetic resonance imaging (MRI) signals (32,33). Here, this algorithm was used to extract power spectral information from one-dimensional electrophysiological signals (voltage vs. time). Use of the LMS-FT allowed enhanced resolution of power-frequency information over time (in our recordings) and proved to be useful for quantifying spectral changes during interictal, preictal, and ictal epochs; effective frequency resolution was set to 4 Hz. This technique circumvents some of the limitations of the classic short-time Fourier transform (ST-FT) by making use of time windows that scale inversely with the frequency being analyzed (31,34). Therefore lower-frequency oscillations were resolved by using larger time windows, whereas the power spectrum of higher-frequency oscillations was computed by using smaller time windows (Fig. 1B, right). Specifically, the ST-FT exhibits no scaling in the frequency axis and hence frequency resolution is traded off for temporal resolution and vice versa (Fig. 1B, left). The LMS-FT allows time-frequency analysis of signals in their most pure form without the need of prebandpass filtering of the data, a practice that can introduce unwanted signal artifacts and consequently inaccurate power spectral information. The LMS-FT shares some similarities with the continuous wavelet transform in its time-frequency resolution properties. However, a key advantage of this method is its close link to the Fourier domain without the loss of information.

Before power-frequency analysis, each of the recordings was decimated from a 2-KHz sampling rate down to 1 KHz by digitally low-pass-filtering the data at 800 Hz followed by resampling. The LMS-FT was computed in a continuous manner for all episodes (interictal+preictal and ictal recordings). To perform quantitative analysis on the power-frequency information obtained by using LMS-FT, we summed the computed power amplitudes in the frequency direction by using the following frequency bands (in Hz): 0–100 (subripple), 100–200 (ripple), 200–300 (fast ripple1), and 300–400 (fast ripple2). This resulted in four “channels” of continuous power-frequency information, over time, that reflect the amplitude of the

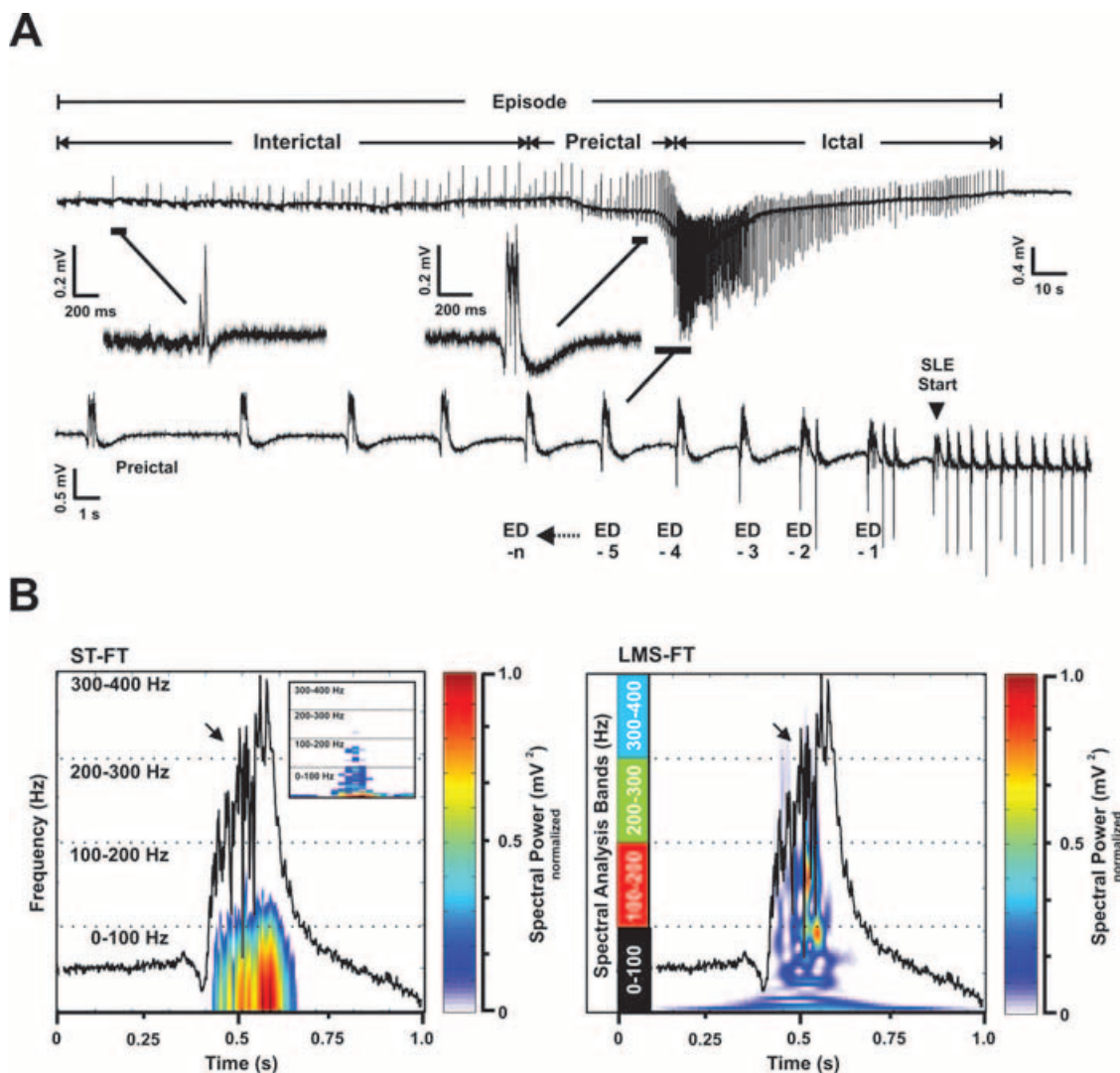


FIG. 1. Transition to seizure activity and analysis of epileptiform and ictal discharges by using power-frequency analysis techniques. **A:** Extracellular recording from the CA1 layer of a hippocampal slice showing the transition from interictal to preictal and then to ictal activity. This is referred to as a single episode (*insets*). Epileptiform discharges (EDs) are numbered backward starting with -1 as the last preictal discharge. The start of seizure begins with discharge zero (*arrowhead*). **B:** Power-frequency analysis of a single epileptiform discharge (*black overlaid trace*) from a different slice. The discharge's power spectrum, in time and frequency (in the range of 0–400 Hz), is shown with power amplitude coded in color, with time and frequency on the x- and y- axes, respectively. **Left:** To obtain good time resolution with using the short-time Fourier transform (ST-FT), analysis must be performed by using small time windows. This compromises the frequency resolution for fast events (*arrowhead*; inset). This can be alleviated by using larger time windows, which sacrifices the temporal resolution. **Right:** Use of the multiscale Fourier transform (LMS-FT) allows optimal time-frequency resolution by using a window size that varies inversely with the frequency. This provides an improvement in time-frequency resolution of high-frequency oscillations (HFOs; *arrowhead*). Analysis parameters were kept fixed for both techniques. The power spectral amplitude is normalized to a maximum of 1, and frequency resolution in the y-axis is 128 points (~ 4 Hz) for both techniques.

power spectrum in each of the four frequency bands. These equally spaced bands were selected to process all conventional (EEG, ~ 0 –100 Hz) low-frequency bands together and to control cumulative power amplitude in each band for group statistical comparison. With this analysis, signal components >400 Hz were ~ 20 times smaller in (power) amplitude relative to lower frequencies. Therefore we considered the full effective bandwidth of our signal (0–400 Hz) for all subsequent time-frequency analyses.

The time at which interictal, preictal, and ictal discharges occur varied from episode to episode and between

different slices. Given that we observed no statistical correlation between the number of discharges leading to seizure and episode number in any of the slices (Pearson's product-moment, $r = -0.46$; $p > 0.05$), we elected to use the start of the seizure as a defined relative time point from which to measure all discharges preceding and also during the actual seizure event. This strategy also was used to allow subsequent direct statistical group analysis of the power-frequency information in relation to preictal changes that may exist before seizure onset. Therefore epileptiform discharges were numbered in the

negative direction, starting from -1 as the first epileptiform discharge (Fig. 1A). Similarly, ictal discharges were numbered in the positive direction, starting with zero as the marker for the seizure start time (Fig. 1A). All discharges were identified manually by visual inspection of all recordings.

The next step in analysis was the precise quantification and statistical comparison of preictal changes in power–frequency information and how these changes evolve from episode to episode. We therefore computed the relative power spectral contribution of each of the computed frequency channels for each discharge by using the start of the seizure as a defined reference point. This group statistical comparison was performed for all 35 episodes by using a linear general model (LGM). A repeated measures analysis of variance (ANOVA) was used to quantify possible temporal trends across discharges and episodes in relation to each of the four frequency bands. Independent variables used in the ANOVA model were episode number and discharge number. Although we computed the continuous power–frequency information for all recordings and the power spectral makeup of each discharge, we restricted the use of the repeated measures ANOVA to the 12 discharges immediately preceding seizure onset that were common to all 35 episodes. In other words, 12 discharges (i.e., EDs) back from the start of seizure was the largest number of discharges common to all recordings. We analyzed all ictal discharges and computed a similar ANOVA matrix for 12 ictal discharges for symmetrical investigation of periictal frequency changes in time. All frequency analyses were performed by using MATLAB (MathWorks Inc. Natick, MA, U.S.A.) and statistical comparisons, by using SPSS (SPSS Inc.). A value of $p \leq 0.05$ was considered significant. Mean values are reported plus/minus the standard error of the mean (SEM). Development and data processing were performed on a Linux-based PC. The WestGrid computing facility (University of Calgary) was used for batch data processing.

RESULTS

Five or more episodes were recorded from each of the seven slices that developed SLEs spontaneously. The mean interepisode time was 3 min (SD, 2). The mean peak amplitude of the stimulus-evoked responses was fairly constant between episodes and, after the fifth SLE, was $94 \pm 5\%$ of the control value measured at the start of the low- Mg^{2+} perfusion. All pre-seizure discharges were analyzed. To assess whether any trends existed in epochs far from the time of transition to seizure, episodes that exhibited >12 EDs ($n = 30$, 85%) were analyzed. No statistically significant differences or trends in the power spectral amplitude of successive discharges were observed for any of the frequency bands ($p = 0.5$). Figure 2A shows such a recording for the first 30 s of a 200-s interictal epoch in an episode

from one slice. The LMS-FT of discharges far from the preictal epoch consistently had low-amplitude power values, as visualized by the color map and discharge plot (Fig. 2A). Figures 2B and C show preictal and ictal discharges taken from a single episode from a different slice. The continuous LMS-FT was computed, and values corresponding to the power spectral makeup of all EDs are shown in the power spectral composition plot (Fig. 2b and c). A gradual increase in the power amplitude of the ripple (100–200 Hz) and FR1 (200–300 Hz) spectral bands was observed for successive discharges leading up to the SLE (Fig. 2B). The insets show the detailed time–frequency morphology of the first two [i] and last two [ii] epileptiform discharges (Fig. 2B, right). These panels also show the increase in the ripple and FR components of these waveforms just before SLE initiation. Analysis of the seizure shows that high frequencies can persist and fluctuate throughout the SLE (Fig. 2C). Notably, the contribution of ripple and FR1 bands to the power-spectral amplitude of each ictal discharge is consistently larger than that of other bands during seizure onset and remains fairly constant over the observed time course (Fig. 2C).

To explore temporal interactions between different neighboring recordings sites, for slices where dual extracellular recordings were available, “running” cross-correlograms were computed between the two channels over time (CA3/CA3 or CA3/CA1). The cross-correlation was computed in 1-s segments of the continuous data, and a lag time of -100 to $+100$ ms was explored. The computed cross-correlation matrix was normalized to the global maximal correlation index between the two signals. This analysis revealed a strong interaction between CA1/CA3 and local CA3/CA3 recording sites during the preictal epoch (Fig. 3). This interaction occurred during the same time period when increasing ripple and FR1 power amplitudes were observed (~ 20 – 30 s) before seizure onset.

We next determined whether the power spectral makeup of epileptiform and ictal discharges followed a trend either over the course of a single episode or between episodes. Table 1 shows a summary of the repeated measures ANOVA analysis for all 35 episodes as computed for 12 discharges before and after seizure initiation (i.e., periictally). The summed amplitude spectrum for all four bands was not different for discharges across different episodes (Table 1). This suggests that no significant changes in the frequency content of preictal and ictal discharges were seen across successive SLEs. However, when the trend across successive discharges was examined during the preictal epoch leading up to each seizure (by collapsing the data across episodes), the amplitude of ripple and FR1 bands were found to be significantly different, on average, from one discharge to the next (ANOVA; $p = 0.006$ and $p = 0.004$, respectively); this was not observed for the low-frequency band ($p = 0.2$). Trend analysis showed

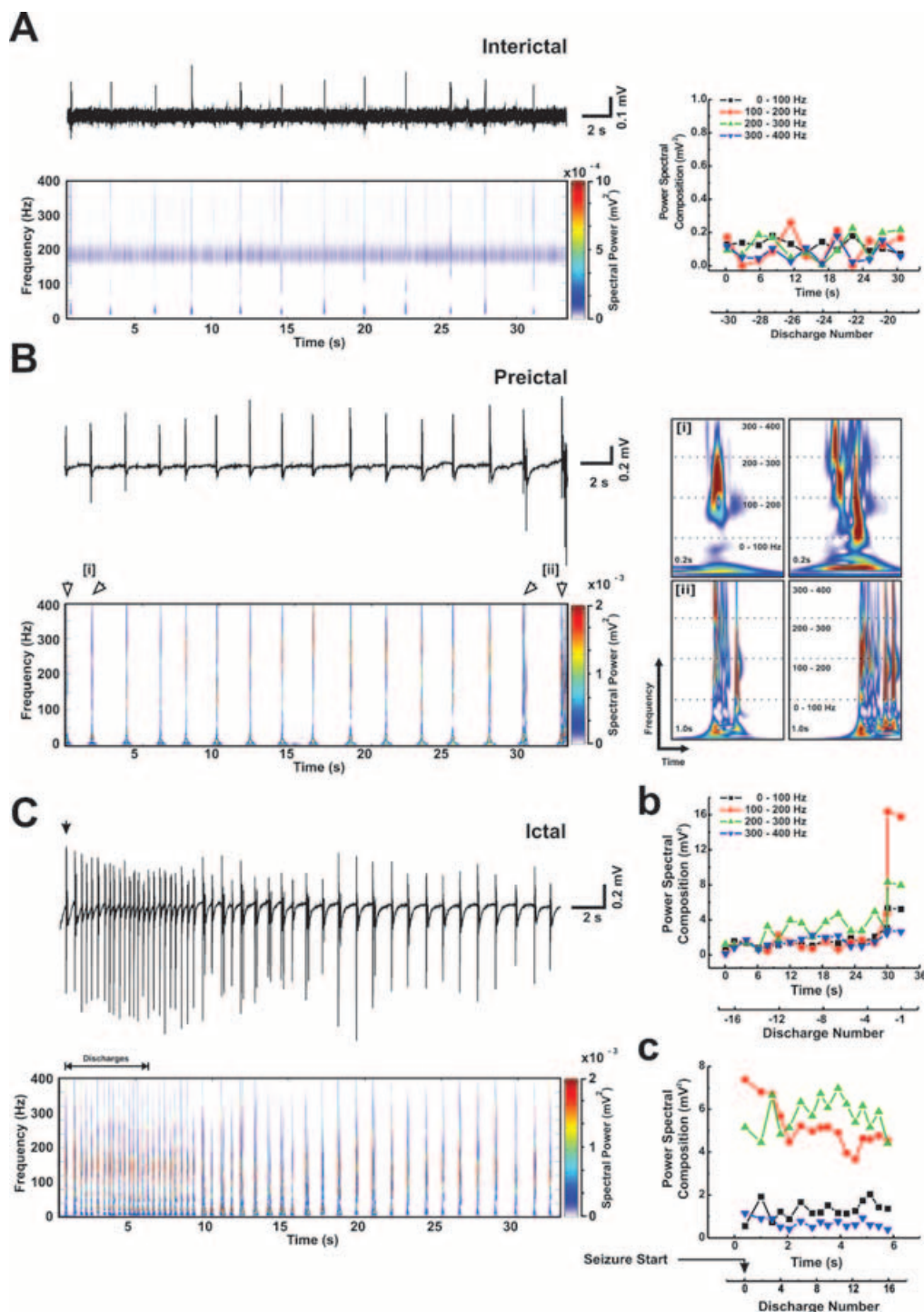


FIG. 2. Power-frequency analysis over time for interictal, preictal, and ictal activity recorded from the CA1 layer of hippocampal slices. **A: Left:** Power analysis of interictal activity for an epoch far from seizure onset. Horizontal bands (*light blue*) on the time-frequency plot correspond to residual power in notch-filtered frequencies, given the low signal-to-noise ratio. **Right:** Discharges are typified by small power-amplitude values for each frequency band without any observable trends. **B: Left:** Epileptiform (interictal-to-preictal) activity recorded from a different slice exhibiting 17 discharges before seizure onset. **Right insets:** Detailed time-frequency morphology of the first two [i] and last two [ii] epileptiform discharges (*hollow arrowheads*). **b:** Power-amplitude composition plot for each epileptiform discharge, showing an increasing trend for ripple and fast-ripple1 (FR1) frequency bands leading up to seizure onset. **C: Left:** Ictal discharges immediately after the activity in **B**; seizure onset is marked by a *solid arrowhead* corresponding to discharge number zero. **c:** Variability is observed in all four frequency bands for ictal discharges. The FR1 (200–300 Hz) band is on average greater in magnitude than the ripple band (100–200 Hz) during the early phase of seizure activity. Power spectral makeup of each discharge, in the four frequency bands, was computed by collapsing and summing the continuous power-frequency values in the frequency direction (see Methods). Discharge time and number are reported for the power-amplitude composition plots (**b** and **c**). Absolute power amplitude is color coded.

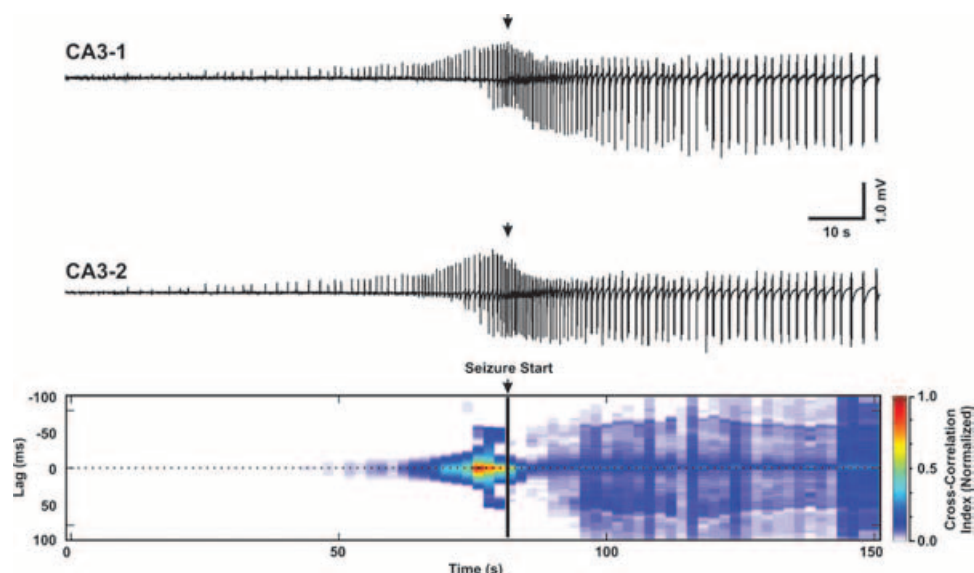


FIG. 3. Simultaneous dual extracellular recording and cross-correlation analysis for two neighboring sites in the CA3 cell layer. Cross-correlation was computed in 1-s windows with a lag of -100 to $+100$ ms. A strong correlation value is observed during an epoch lasting ~ 25 s, corresponding to the preictal period before seizure onset. A strong correlation between the two signals, albeit smaller in relative magnitude, is observed throughout the seizure event (*bright region* about zero lag). The correlation matrix was normalized to a maximum of 1 in relation to the maximal correlation index for the entire episode.

a linear increase in the power spectral amplitudes corresponding to the low-frequency band (0–100 Hz; $p = 0.05$) as well as both ripple and FR1 bands over time ($p = 0.01$ for both). This robust increase, with discharge number, is shown in Fig. 4A for all 35 pre seizure recordings. It is intriguing to note that although different episodes exhibited different numbers of EDs, the absolute power amplitude in each band remained in proportion to the mean power at that discharge number. For example, although 75% of the pre seizure recordings exhibited ≤ 15 discharges (inset, Fig. 4A), discharges close to the preictal period had elevated low-frequency power amplitudes (0–100 Hz) in accordance with the trend observed in episodes that had ≤ 30 EDs (note that SEM values remain fairly constant over the range of discharges).

Analysis of ictal discharges did not show any significant increasing or decreasing trends either across discharges in a single seizure or across seizures in successive episodes (Fig. 4B and Table 1). However, ripple and FR1 composed a dominant component of the power spectral amplitude during the initial phase of the seizure but fluctuated over its course (Fig. 4B, left). The accumulation of power amplitudes in these bands can also be visualized in an alternative manner (Fig. 4B, right).

For preictal activity (Fig. 4A, right), the normalized (mean) cumulative sum for each band showed that ripple and FR1 bands gain more of their amplitude during the last few discharges before SLE onset (corresponding to ~ 20 s preictally). Comparatively, the start of the SLE (Fig. 4B, right) was characterized by a comparable

TABLE 1. Statistical analysis results for epileptiform and ictal discharges in each of the four spectral bands

Frequency band	Within-subject (slice) test	Interictal/Preictal		Ictal	
		ANOVA	(Linear) Trend analysis	ANOVA	(Linear) Trend analysis
0–100 Hz	Episodes	$p = 0.7$	$p = 0.9$	$p = 0.5$	$p = 0.7$
	Discharges	$p = 0.2$	$p = 0.05$	$p = 0.5$	$p = 0.6$
100–200 Hz	Episodes	$p = 0.4$	$p = 0.7$	$p = 0.3$	$p = 0.8$
	Discharges	$p = 0.006$	$p = 0.01$	$p = 0.4$	$p = 0.4$
200–300 Hz	Episodes	$p = 0.4$	$p = 0.9$	$p = 0.4$	$p = 0.7$
	Discharges	$p = 0.004$	$p = 0.01$	$p = 0.5$	$p = 0.2$
300–400 Hz	Episodes	$p = 0.5$	$p = 0.6$	$p = 0.3$	$p = 0.8$
	Discharges	$p = 0.2$	$p = 0.07$	$p = 0.5$	$p = 0.3$

Repeated measures analysis of variance, p values are shown for comparing the power spectral information with respect to differences of means across Discharges or across Episodes. For example, for Discharges, the p value represents the probability of accepting the null hypothesis: that there are no differences in the means of neighboring discharge's power spectral amplitude for a particular band when considering all of the discharges. Additional p values also are cited for compliance with the existence of a linear trend. Significance is considered for $p \leq 0.05$ (italicized values).

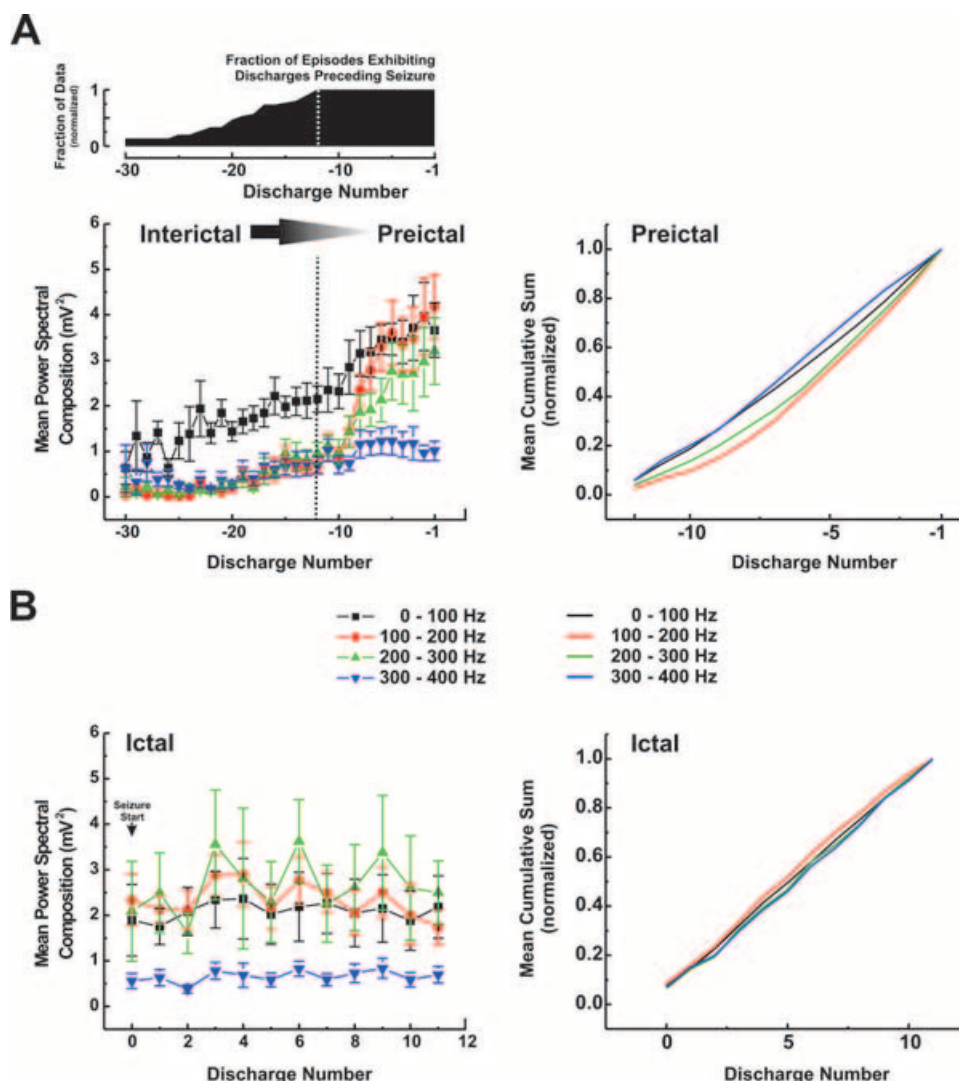


FIG. 4. Temporal evolution of the mean power spectral amplitude, in each frequency band, for individual discharges during epileptiform (interictal and preictal) and ictal activity. **A: Left:** Mean power-amplitude composition plot for all epileptiform discharges. During the preictal epoch, the amplitude of the 0- to 100-Hz band increases linearly with discharge number at a rate of change (least squares slope, $m = 0.16$) that is smaller in magnitude in relation to the ripple and FR1 bands ($m = 0.36$ and $m = 0.21$, respectively). During the preictal period, a marked increase is seen in ripple (100–200 Hz) and fast ripple1 (200–300 Hz) frequency makeup for each of the discharges. **Inset, top left:** The fraction of data, for all episodes ($n = 35$, $n = 7$ slices), that exhibited discharges preceding seizure onset. All episodes had ≥ 12 pre-seizure epileptiform discharges and $\sim 25\%$ of all episodes recorded exhibited >20 discharges. Repeated measures analysis of variance (ANOVA) analysis of the activity present in all episodes (last 12 pre-seizure discharges) revealed a linear trends for the 0- to 100-Hz ($p = 0.05$) and also the ripple and FR1 bands ($p = 0.01$ for both). **Right:** Normalized mean cumulative sum of the power amplitudes, in each of the four bands, for discharges subjected to repeated measures ANOVA analysis. The low-frequency (0–100 Hz) and fast-ripple2 (300–400 Hz) bands accumulate linearly, whereas the ripple and FR1 bands (100–300 Hz) gain most of their spectral magnitude during the last six discharges preceding the seizure. **B: Left:** Mean power-amplitude composition plot for ictal discharges during the immediate epoch of seizure activity. A great deal of variability is present in the power spectral successive discharges, with the greatest contribution made by the power amplitude of the FR1 band. **Right:** Normalized (mean) cumulative sum for each of the spectral bands during the early phase of seizure activity for all 35 episodes. All bands seem to gain their power amplitudes together and at an equal rate. When these data were analyzed in relation to changes from one episode to the next, no statistically significant (linear) trends were observed for epileptiform or ictal discharges. For both plots (top row), data are nonscaled and nonnormalized; all values expressed as mean \pm SEM for the error bars.

increase across all four spectral bands with close superposition of the cumulative power amplitude curves for each band. No statistically significant differences were observed between the power spectral trends computed for recordings obtained from CA1 versus CA3 pyramidal cell layers ($p > 0.9$; t test).

DISCUSSION

We investigated the temporal dynamics of HFOs and demonstrated distinct changes in ripple and FR activity during the transition (preictal) to seizure onset. We have shown that the spectral composition of epileptiform discharges changes, increasing in a time-dependent manner,

leading up to seizure onset. This increasing linear trend in power spectral amplitude was statistically significant for low frequencies (0–100 Hz; $p = 0.05$) as well as for ripple (100–200 Hz) and FR1 (200–300 Hz) frequency bands ($p = 0.01$; $n = 35$). The preictal period was consistently observed to exhibit strong differences in relation to discharge number, gaining power spectral amplitude toward the time of seizure onset in ripple and FR1 frequency bands ($p = 0.006$ and $p = 0.004$, respectively). No such increase (or decrease) was observed during ictal activity or when pre-seizure and seizure discharges were compared across successive seizure episodes ($p \geq 0.3$). Furthermore, no trends were observed for any of the frequency bands during the early phase of interictal activity ($p \geq 0.5$; $n = 30$).

The specific association of FRs with abnormal (epileptiform) activity has been explored in both rodents and humans. Evidence from previous studies suggests that FRs are restricted to areas adjacent to lesioned kainic acid injection sites *in vivo* (6) and occur more frequently ipsilateral to seizure-onset regions in epilepsy patients (5,8,20). Specifically, FRs have been found in association with epileptic brain tissue in humans with mesial temporal lobe epilepsy (5), with and without hippocampal atrophy (35), and also in the entorhinal cortex (8). These findings may reflect the presence of pathologically interconnected clusters of neurons that are active well before the manifestation of spontaneous behavioral seizures (36).

Our findings are consistent with the presence of HFOs occurring during interictal activity. Furthermore, we have shown that although low-frequency activity (0–100 Hz) increases linearly toward the time of seizure onset, it is the transient and sharp increase in ripple and fast ripples (of 100–300 Hz) that is a characteristic feature of the transition to the ictal state in this model of epilepsy (Fig. 2B and C). Examination of temporal correlations between different spatial sites (e.g., CA3/CA3 or CA3/CA1) recorded within the slice during epileptic activity revealed strong interactions that take place preictally (~ 20 s before seizure onset), which match the time epoch during which increases in HFO activity were observed (Fig. 3). This interaction may be interpreted as synchronization processes common to both phenomena. However, it should be noted that cross-correlation analyses identify a relation between signals but do not necessarily provide information about the local timing of that interaction. In other words, our findings suggest that signals are strongly correlated on the order of a lag equal to $\tau = 10$ –25 ms (Fig. 3). However, we cannot directly relate this to the time-scale in which the cellular elements participating in ripple/FR activity are acting to result in putative neuronal synchronization during the preictal period. Indeed, HFO activity is believed to be a local phenomenon (36), and as such, to address properly the local time-scale of synchronization between individual neurons, high-impedance multisite recordings

are required (e.g., using silicon-based multielectrode arrays).

Patient-based studies have described HFOs during interictal activity in the range of 80–500 Hz, with the majority of discharges exhibiting oscillations at 100 Hz (ripple) and 250 Hz (FR), and with 90% of FR activity occurring within 186–392 Hz (20,36). We have observed HFOs over a similar frequency range, except that the power amplitude of frequencies >400 Hz were ~ 20 times smaller and did not exhibit detectable temporal trends on statistical analyses. However, we acknowledge the challenge of relating *in vitro* experimental findings to findings in epilepsy patients. Clinically, resection of parahippocampal structures (e.g., entorhinal cortex, subiculum), which also are believed to be involved in FR generation, is correlated with improved seizure control (37,38). This implies that neuronal networks involved in HFO generation are both localized to and extend beyond the hippocampus proper.

Two previous *in vitro* studies observed preictal changes in HFOs. One study used extracellular recordings in areas CA1, CA3, and the dentate gyrus in rat hippocampal slices exposed to either high-potassium or 4-aminopyridine (23). The classic Fourier transform technique was used to analyze EDs for 4 min leading up to a seizure, and a gradual increase in low-frequency (2–40 Hz) and FR (200–400 Hz) activity was seen in some slices, but variability of this effect was reported as large. Another study used a zero-magnesium model of recurrent seizures and performed extracellular and intracellular voltage- and current-clamp recordings of CA3 pyramidal cells (24). Two large spectral bands spanning 50–400 Hz and 400–800 Hz were analyzed by using a wavelet technique and quantified by using a power-like quantity: “HFO energy.” A progressive increase in HFO energy was observed in 400–800 Hz, restricted to the immediate transition epoch to seizure onset, although not reported as statistically significant. However, they noted an increasing component with dominant frequencies at 100 and 300 Hz for several discharges preceding seizure onset. Therefore although reported as not statistically significant, the increasing trends observed in these studies are consistent with the increases we have described. Notably, the aforementioned studies revealed trends in different HFO frequency components before seizure onset. We likely obtained statistical significance because we used narrower-frequency bands for analysis, thereby increasing statistical power. Another factor might be that the previous studies used different chemical manipulations to provoke seizures (i.e., zero Mg^{2+} , high K^+ , and 4-aminopyridine vs. low Mg^{2+} , in addition to differences in the age of animals).

The mechanisms underlying ripples and FRs are incompletely understood. Under nonepileptic conditions, recordings in the CA1 layer of the hippocampus in active and anesthetized rats have implicated dynamic network interactions involving interneurons and pyramidal

cells as possible causes for ripples (4). Blockage of excitatory (glutamatergic) and inhibitory (γ -aminobutyric acid; GABA_A) synaptic transmission can also modulate HFOs in both normal and epileptic conditions (10,23). It has been shown that, in the neocortices of cats, rapid spiking from subpopulations of neuronal networks can cause ripples, which can be associated with seizure initiation (39,40). Another study showed that high-frequency (200–800 Hz) activity was present in extracellular recordings and that this activity correlated with fast components present in voltage-clamp currents in CA3 neurons, during the transition from interictal to ictal activity, in hippocampal slices exposed to zero magnesium (24). This suggests that high-frequency inputs onto pyramidal neurons contribute to HFO activity in the zero-magnesium model of epilepsy. They reported that actual pyramidal cell-firing rates never reached such high frequencies as those detected extracellularly or in intracellular voltage-clamp recordings. This raises the possibility that anti- and orthodromic axonal firing may also be involved (41).

Synchronization via gap junctions also is implicated in the generation of HFOs in normal and epileptic conditions. Studies using hippocampal slices suggest that interneuronal electrical coupling, in the form of axonal connectivity, is required for HFOs (14,42). A reduction in spontaneous sharp waves and ripple oscillations in connexin-36 mice has also been reported (43), implicating gap junctions in ripple generation (11). In addition, halothane and other gap-junctional blockers such as carbenoxolone are known to have inhibitory effects on both ripples and FRs (4,13,44). Taken together, these data suggest that both synaptic and nonsynaptic mechanisms participate in dynamic alterations in synchronous inputs onto and between pyramidal neurons in the hippocampus during the transition to ictal activity.

The fact that pyramidal cell firing rates do not reach FR frequencies suggests that temporal and spatially dynamic interactions in epileptic neuronal networks, or interneuronal firing activity per se, are important mechanisms underlying fast oscillations. When recorded extracellularly, these modalities of communication combine to form complex, but analyzable, waveforms. Based on the link between FR oscillations and an underlying epileptic condition, characterization of HFOs may contribute to the understanding of dynamics present in epileptic neuronal networks (45). Robust detection and visualization of HFOs may also provide insights into localization of epileptic foci and aid in the detection of characteristic electrophysiologic changes that precede seizures.

Acknowledgment: We are grateful to the following funding agencies for their support: H.K. is supported by studentships from Natural Sciences and Engineering Research Council of Canada (NSERC, CGS) and the Alberta Heritage Foundation for Medical Research (AHFMR). J.R.M. is supported by grants awarded from the Multiple Sclerosis Society of Canada and

AHFMR. B.L.B. is supported by a grant awarded from NSERC; P.F., by grants awarded from AHFMR and the Canadian Institutes for Health Research (CIHR); and P.L.C., by grants awarded from CIHR and the CURE (Citizens United for Research in Epilepsy) Foundation.

We thank Dr. Michael Eliasziw, Jodi Edwards, and Dr. Bradley Goodyear for their helpful comments regarding statistical analysis of the data.

REFERENCES

1. Traub RD, Jefferys JGR, Whittington MA. *Fast oscillations in cortical circuits*. Cambridge, Mass: MIT Press, 1999.
2. Buzsaki G, Horvath Z, Urioste R, et al. High-frequency network oscillation in the hippocampus. *Science* 1992;256:1025–7.
3. Chrobak JJ, Buzsaki G. Selective activation of deep layer (V-VI) retrohippocampal cortical neurons during hippocampal sharp waves in the behaving rat. *J Neurosci* 1994;14:6160–70.
4. Ylinen A, Bragin A, Nadasdy Z, et al. Sharp wave-associated high-frequency oscillation (200 Hz) in the intact hippocampus: network and intracellular mechanisms. *J Neurosci* 1995;15:30–46.
5. Bragin A, Engel J Jr, Wilson CL, et al. High-frequency oscillations in human brain. *Hippocampus* 1999;9:137–42.
6. Bragin A, Engel J Jr, Wilson CL, et al. Hippocampal and entorhinal cortex high-frequency oscillations (100–500 Hz) in human epileptic brain and in kainic acid-treated rats with chronic seizures. *Epilepsia* 1999;40:127–37.
7. Bragin A, Mody I, Wilson CL, et al. Local generation of fast ripples in epileptic brain. *J Neurosci* 2002;22:2012–21.
8. Bragin A, Wilson CL, Staba RJ, et al. Interictal high-frequency oscillations (80–500 Hz) in the human epileptic brain: entorhinal cortex. *Ann Neurol* 2002;52:407–15.
9. Fisher RS, Webber WR, Lesser RP, et al. High-frequency EEG activity at the start of seizures. *J Clin Neurophysiol* 1992;9:441–8.
10. Maier N, Nimmrich V, Draguhn A. Cellular and network mechanisms underlying spontaneous sharp wave-ripple complexes in mouse hippocampal slices. *J Physiol* 2003;550:873–87.
11. Draguhn A, Traub RD, Schmitz D, et al. Electrical coupling underlies high-frequency oscillations in the hippocampus in vitro. *Nature* 1998;394:189–92.
12. Bikson M, Fox JE, Jefferys JG. Neuronal aggregate formation underlies spatiotemporal dynamics of nonsynaptic seizure initiation. *J Neurophysiol* 2003;89:2330–3.
13. Cunningham MO, Halliday DM, Davies CH, et al. Coexistence of gamma and high-frequency oscillations in rat medial entorhinal cortex in vitro. *J Physiol* 2004;559:347–53.
14. Traub RD, Draguhn A, Whittington MA, et al. Axonal gap junctions between principal neurons: a novel source of network oscillations, and perhaps epileptogenesis. *Rev Neurosci* 2002;13:1–30.
15. Traub RD, Schmitz D, Jefferys JG, et al. High-frequency population oscillations are predicted to occur in hippocampal pyramidal neuronal networks interconnected by axoaxonal gap junctions. *Neuroscience* 1999;92:407–26.
16. Traub RD, Whittington MA, Buhl EH, et al. A possible role for gap junctions in generation of very fast EEG oscillations preceding the onset of, and perhaps initiating, seizures. *Epilepsia* 2001;42:153–70.
17. Buzsaki G. Memory consolidation during sleep: a neurophysiological perspective. *J Sleep Res* 1998;7(suppl 1):17–23.
18. Siapas AG, Wilson MA. Coordinated interactions between hippocampal ripples and cortical spindles during slow-wave sleep. *Neuron* 1998;21:1123–8.
19. Bragin A, Wilson CL, Engel J. Spatial stability over time of brain areas generating fast ripples in the epileptic rat. *Epilepsia* 2003;44:1233–7.
20. Staba RJ, Wilson CL, Bragin A, et al. High-frequency oscillations recorded in human medial temporal lobe during sleep. *Ann Neurol* 2004;56:108–15.
21. Bragin A, Wilson CL, Almajano J, et al. High-frequency oscillations after status epilepticus: epileptogenesis and seizure genesis. *Epilepsia* 2004;45:1017–23.

22. Litt B, Lehnertz K. Seizure prediction and the pre seizure period. *Curr Opin Neurol* 2002;15:173–7.
23. Dzhala VI, Staley KJ. Transition from interictal to ictal activity in limbic networks in vitro. *J Neurosci* 2003;23:7873–80.
24. Lasztocki B, Antal K, Nyikos L, et al. High-frequency synaptic input contributes to seizure initiation in the low-[Mg²⁺] model of epilepsy. *Eur J Neurosci* 2004;19:1361–72.
25. Worrell GA, Parish L, Cranstoun SD, et al. High-frequency oscillations and seizure generation in neocortical epilepsy. *Brain* 2004;127:1496–506.
26. Rafiq A, DeLorenzo RJ, Coulter DA. Generation and propagation of epileptiform discharges in a combined entorhinal cortex/hippocampal slice. *J Neurophysiol* 1993;70:1962–74.
27. Rafiq A, Zhang YF, DeLorenzo RJ. Long-duration self-sustained epileptiform activity in the hippocampal-parahippocampal slice: a model of status epilepticus. *J Neurophysiol* 1995;74:2028–42.
28. Mody I, Lambert JD, Heinemann U. Low extracellular magnesium induces epileptiform activity and spreading depression in rat hippocampal slices. *J Neurophysiol* 1987;57:869–88.
29. Traub RD, Jefferys JG, Whittington MA. Enhanced NMDA conductance can account for epileptiform activity induced by low Mg²⁺ in the rat hippocampal slice. *J Physiol* 1994;478:379–93.
30. Gutierrez R, Armand V, Schuchmann S, et al. Activity induced by low Mg²⁺ in cultured rat hippocampal slices. *Brain Res* 1999;815:294–303.
31. Pinnegar CR, Mansinha L. The S-transform with windows of arbitrary and varying shape. *Geophysics* 2003;68:381–5.
32. Goodyear BG, Zhu H, Brown RA, et al. Removal of phase artifacts from fMRI data using a Stockwell transform filter improves brain activity detection. *Magn Reson Med* 2004;51:16–21.
33. Zhu H, Goodyear BG, Lauzon ML, et al. A new local multiscale Fourier analysis for medical imaging. *Med Phys* 2003;30:1134–41.
34. Hilfiker P, Egli M. Detection and evolution of rhythmic components in ictal EEG using short segment spectra and discriminant analysis. *Electroencephalogr Clin Neurophysiol* 1992;82:255–65.
35. Staba RJ, Wilson CL, Bragin A, et al. Quantitative analysis of high-frequency oscillations (80–500 Hz) recorded in human epileptic hippocampus and entorhinal cortex. *J Neurophysiol* 2002;88:1743–52.
36. Bragin A, Wilson CL, Engel J Jr. Chronic epileptogenesis requires development of a network of pathologically interconnected neuron clusters: a hypothesis. *Epilepsia* 2000;41(suppl 6):S144–52.
37. Abosch A, Bernasconi N, Boling W, et al. Factors predictive of suboptimal seizure control following selective amygdalohippocampectomy. *J Neurosurg* 2002;97:1142–51.
38. Siegel AM, Wieser HG, Wichmann W, et al. Relationships between MR-imaged total amount of tissue removed, resection scores of specific mediobasal limbic subcompartments and clinical outcome following selective amygdalohippocampectomy. *Epilepsy Res* 1990;6:56–65.
39. Grenier F, Timofeev I, Steriade M. Focal synchronization of ripples (80–200 Hz) in neocortex and their neuronal correlates. *J Neurophysiol* 2001;86:1884–98.
40. Grenier F, Timofeev I, Steriade M. Neocortical very fast oscillations (ripples, 80–200 Hz) during seizures: intracellular correlates. *J Neurophysiol* 2003;89:841–52.
41. Gutnick MJ, Prince DA. Thalamocortical relay neurons: antidromic invasion of spikes from a cortical epileptogenic focus. *Science* 1972;176:424–6.
42. Traub RD, Bibbig A, LeBeau FE, et al. Cellular mechanisms of neuronal population oscillations in the hippocampus in vitro. *Annu Rev Neurosci* 2004;27:247–8.
43. Maier N, Guldenagel M, Sohl G, et al. Reduction of high-frequency network oscillations (ripples) and pathological network discharges in hippocampal slices from connexin 36-deficient mice. *J Physiol* 2002;541:521–8.
44. Nimmrich V, Maier N, Schmitz D, et al. Induced sharp wave-ripple complexes in the absence of synaptic inhibition in mouse hippocampal slices. *J Physiol* 2005;563:663–70.
45. Lopes da Silva F, Blanes W, Kalitzin SN, et al. Epilepsies as dynamical diseases of brain systems: basic models of the transition between normal and epileptic activity. *Epilepsia* 2003;44(suppl 12):72–83.